Available online at www.sciencedirect.com
ScienceDirect
Radiation Measurements 43 (2008) 1226–1230
Radiation Measurements
www.elsevier.com/locate/radmeas

Neutron induced alpha radiography

M.A. Stanojev Pereira, R. Pugliesi*, F. Pugliesi

Instituto de Pesquisas Energeticas e Nucleares (IPEN-CNEN/SP), Av. Prof. Lineu Prestes 2242, Cidade Universitária, Butantã, CEP 05508-000 São Paulo, SP, Brazil

Received 18 May 2007; received in revised form 12 December 2007; accepted 18 February 2008

Abstract

A radiography technique which makes use of α-particles as penetrating radiation has been developed. The images were registered in the solid-state nuclear track detector CR-39 and the conditions to obtain the best radiography image were 2.2 h of irradiation and 25 min of etching in a KOH (30%) aqueous solution at 70 °C. For such conditions the resolution in the image was 23 μm. Some radiographs are shown and demonstrate the potential of the technique to inspect samples with thickness in the μm range.
© 2008 Elsevier Ltd. All rights reserved.

Keywords: Neutron converter; Thin layers; Detection limits

1. Introduction

Neutron induced alpha radiography (NIAR) is a non-destructive testing technique which makes use of a low energy α-particles field as penetrating radiation to inspect the internal structure of thin sample layers of the order of few μm (Pugliesi, 2001). This technique has demonstrated to be suitable to inspect, for example, documents and biological samples. The source of the particles is a boron screen which under irradiation with thermal neutrons provides alphas with energy of 1.47 MeV. The film used to register the images was a solid state nuclear track detector (SSNTD). Radiographs are obtained with an aluminum cassette containing the SSNTD, a sample and the screen (in this order in the direction of the neutron beam) and these constituents are kept in tight contact during neutron irradiation. The neutrons pass through the SSNTD, through the sample and will induce (n, α) reactions in the boron screen. The generated particles reach the sample and the transmitted intensity impinges on the SSNTD. The interaction of the α-particles with the detector leaves a narrow and permanent trail of damages with diameters of about 100 Å and length of about 9 μm, the range of the α-particles in the SSNTD (Durrani and Bull, 1987). Under an adequate chemical etching, the damaged regions being more reactive than the surrounding undamaged areas are enlarged forming permanent tracks, which are responsible for the darkening of the detector and therefore for the image formation (Ilic and Najzer, 1990a).

The SSNTD exhibits two important characteristics for radiography purposes: low intrinsic optical contrast and high intrinsic spatial resolution in the image (Hardt and Roettger, 1981). Since the former is the main restriction to its use in radiography, the evaluation of the experimental conditions to obtain the best contrast in the image and the evaluation of the intrinsic resolution for these same experimental conditions were the main objectives of the present paper. The obtained results were interpreted according to the image formation theory in SSNTD, based on the optical properties of a single track (Ilic and Najzer, 1990a–d) and for such purpose some data regarding the track size behavior as functions of the etching time are also presented.

2. Experimental

The irradiations were performed at the neutron radiography facility installed at the BH8 of the 5MW IEA-R1 nuclear research reactor. The characteristics of the neutron beam at the sample irradiation position are given in Table 1(Pugliesi et al., 2005). The irradiations were performed in the aluminum

* Corresponding author. Tel.: +55 11 3133 9968; fax: +55 11 3133 9960.
E-mail address: pugliesi@ipen.br (R. Pugliesi).

1350-4487/$ - see front matter © 2008 Elsevier Ltd. All rights reserved.
doi:10.1016/j.radmeas.2008.02.012

Table 1
Characteristics of the neutron beam at the sample irradiation position

Thermal neutron flux ($n\,cm^{-2}\,s^{-1}$)	1.05×10^6
Neutron/gamma ratio ($n\,cm^{-2}\,mrem^{-1}$)	$4.4.10^6$
Beam diameter (cm)	22
Mean energy (meV)	7

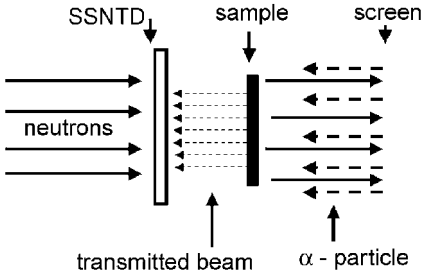

Fig. 1. Setup of the NIAR experiment.

cassette, containing the SSNTD, the sample and the screen. The experimental setup is schematically shown in Fig. 1. The screen is a plastic backing having an overall thickness of about 170 μm (plastic ∼ 105 μm, boron layer ∼ 65 μm) manufactured by Kodak-Pathé, and the SSNTD is the CR-39 (500 μm thickness) manufactured by Pershore moldings. After α-particle exposure the CR-39 was etched in a KOH (30%) aqueous solution at 70 °C (Durrani and Bull, 1987). During the etching, the CR-39 is inserted in a 400 ml glass container containing the solution and this set is immersed in a heated water bed. The darkening level of the CR-39 was determined by quantifying the transmitted light intensity in a 8 bits gray level scale ranging from 0 (darkest pixel) to 255 (brightest pixel) using a light transmission scanner coupled to a computer.

2.1. Best contrast conditions

The contrast is defined as (Hardt and Roettger, 1981):

$$G = \frac{\Delta(GL)}{\Delta \log(E)}. \quad (1)$$

The experimental conditions for the best contrast have been determined from curves that relate gray level (GL) and exposure (E) as functions of the etching time by comparing the values of three parameters:

- The contrast given by the slope of the steeper region of the curves evaluated by Eq. (1).
- The exposure to reach the end of the best contrast region, that is, the exposure for which the detector reaches the highest darkening level.
- The dynamic range corresponding to the best contrast region.

Since the α-particles are generated by neutrons, these curves were obtained as functions of the neutron exposure $E = \phi \cdot t$, where ϕ is the neutron flux ($n \cdot s^{-1} \cdot cm^{-2}$) and t is the irradiation time (s). For such a purpose, several strips of the

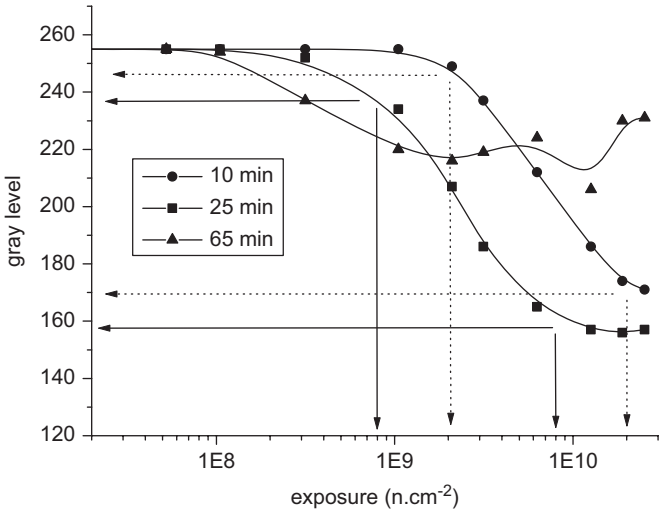

Fig. 2. Gray level as functions of exposure for 10, 25 and 65 min of etching.

Table 2
Radiography parameters for three selected etching times

Etching time (min)	Contrast	Exposure ($n\,cm^{-2}$)	Dynamic range
10	75	2×10^{10}	75
25	80	8×10^9	80
65	26	2×10^9	34

CR-39 were irradiated in the interval $2 \times 10^7\,n\,cm^{-2} < E < 3 \times 10^{10}\,n\,cm^{-2}$ and the resulting gray level intensities for three etching times, 10, 25 and 65 min are shown in Fig. 2. These etching times were selected by taking into account the results obtained in a previous work in which the darkening of the CR-39 was studied in intervals of 5 min, between 10 and 65 min of etching. According to these results, for 10, 25 and 65 min the detector shows the greatest differences in the darkening behavior (Pugliesi et al., 1999).

The obtained values for the three parameters are given in Table 2. Although the curves for 10 and 25 min exhibit nearly the same contrast and dynamic range the selected etching time was 25 min because the required exposure to reach the end of the best contrast region is $E = 8 \times 10^9\,n\,cm^{-2}$ (corresponding to an irradiation of 2.2 h), which is about 2.5 times smaller than the exposure for 10 min.

2.2. Resolution

In radiography, the spatial resolution is defined as the minimal distance that two objects must be separated before they can be distinguished from each other (Ilic and Najzer, 1990d). Since the α-particles are emitted in all directions they will damage the SSNTD over an area greater than the area from which they originate. Therefore, the resolution depends on:

a —the thickness of the sample;
b —the sample to detector distance;
c —the track size;
d —the range of the particles in the SSNTD.

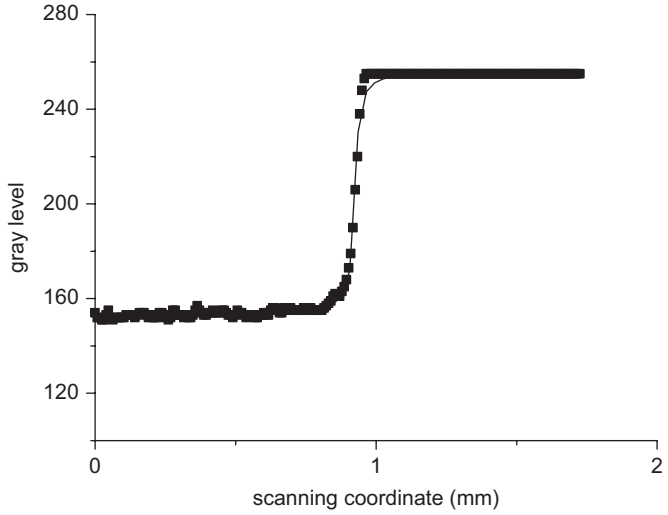

Fig. 3. Gray level intensity distribution and the fitted ESF.

Table 3
Radiography characteristics of the CR-39 (etching time 25 min)

Total unsharpness (μm)	23 ± 1
Inner circle diameter (μm)	1.25 ± 0.05
External ring diameter (μm)	2.55 ± 0.07
External ring area (μm^2)	3.88

The resolution is usually evaluated in terms of the total unsharpness—U_t and results from the combined effect of the geometric unsharpness—U_g (a and b) and of the intrinsic unsharpness—U_i (c and d) (Harms and Zellinger, 1977).

The total unsharpness has been determined from the gray level distribution in the radiography image of an alpha opaque knife-edge object (Mylar foil 10 μm thick), obtained in those same experimental conditions for which the best contrast was achieved, that is, etching time 25 min and exposure of 8×10^9 n cm^{-2}. The image was scanned at 3200 dpi (dots per inch) and the following edge spread function—ESF (Wrobel and Greim, 1988; Harms and Zellinger, 1977) was fitted to the resulting distribution:

$$\mathrm{ESF} = p_1 + p_2 \cdot a \tan(p_3 \cdot (X - p_4)), \quad (2)$$

where X is the distribution spatial coordinate, p_1, p_2, p_3 and p_4, are free parameters and $U_t = 2/(p_3)$.

A typical distribution and the fitting of the ESF to the experimental data are shown in Fig. 3. The obtained value was $U_t = 23$ μm, given in Table 3.

3. Data analysis

According to the image formation theory in SSNTD, a track can be represented by an inner circle surrounded by an external ring as shown in Fig. 4a. The ring is the responsible for the darkening of the detector. When two tracks are overlapped, Fig. 4b, the resulting external ring area is smaller than the sum of the individual areas and consequently the darkening rate is slower. Figs. 5a and b show the behavior of inner circle and external ring diameters as well as of the external ring area for the CR-39 as functions of the etching time and the values for 25 min are given in Table 3 (Pereira, 2007).

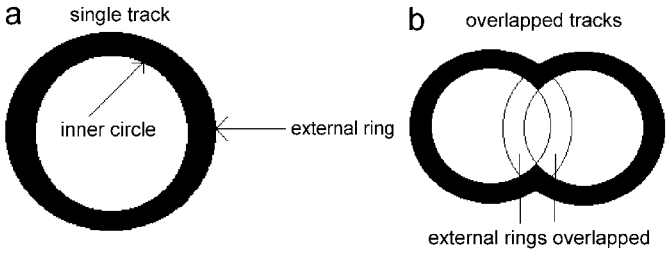

Fig. 4. (a) Schematic representation of a single track; (b) schematic representation of two overlapped tracks.

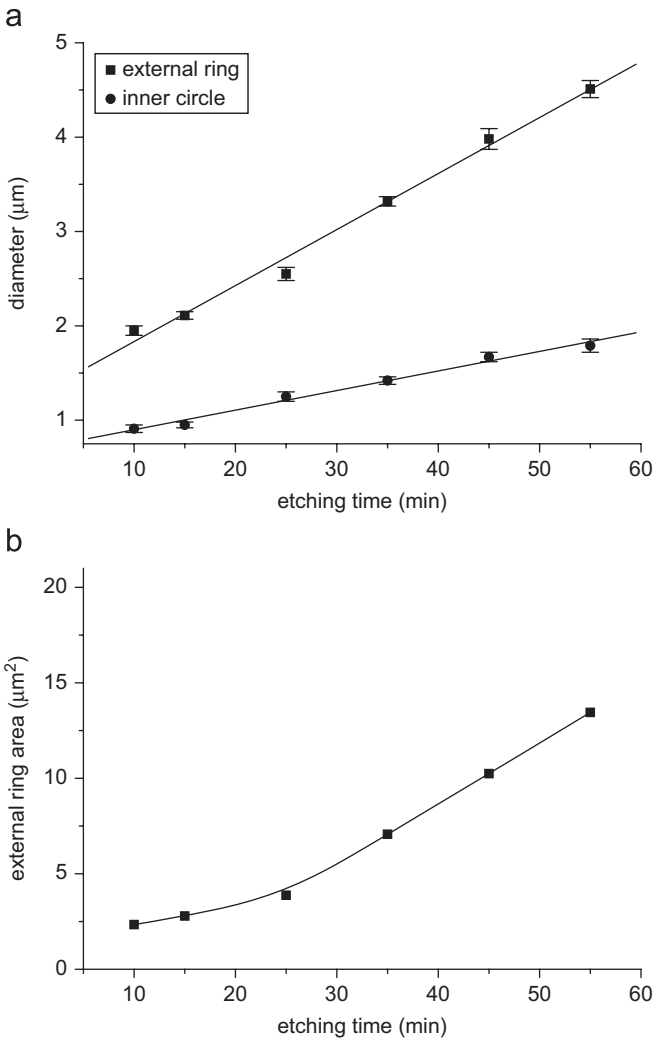

Fig. 5. (a) Behavior of the inner circle and of the external ring diameters as a function of the etching time; (b) external ring area as functions of the etching time.

According to this theory the behavior of the curves for the three studied etching times can be explained as follows. For 25 min, up to the exposure $E \sim 1 \times 10^8$ n cm^{-2}, the track density

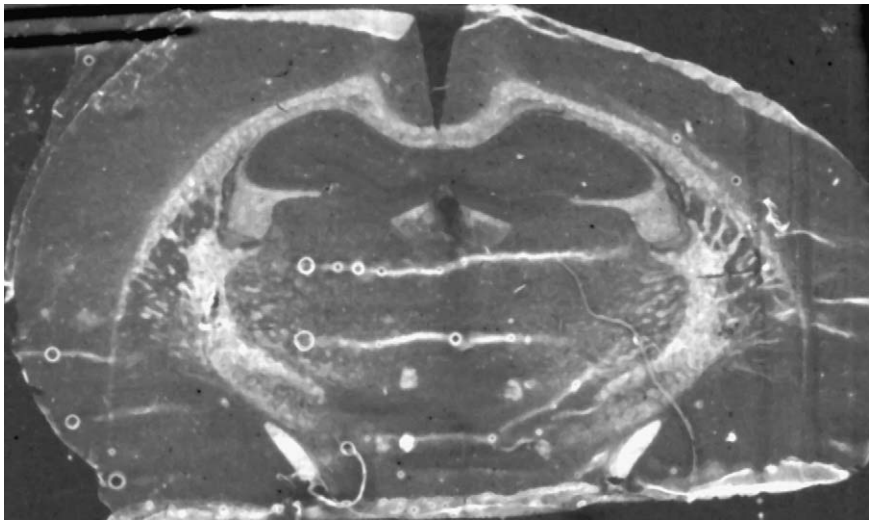

Fig. 6. Radiography of a mice brain tissue (etching 25 min; exposure 8×10^9 n cm^{-2}).

(tr/cm^2) is relatively small and the darkening is negligible. The gray level intensity remains near the detector background (GL $\sim$ 255); for 1×10^8n cm$^{-2} < E < 8 \times 10^8$n cm^{-2} an increase of the exposure is accompanied by an increase of the darkening; however, the track density is still small to produce appreciable darkening; for 8×10^8 n cm$^{-2} < E < 8 \times 10^9$ n cm^{-2} the track density is appreciable and the single track production overcomes the track overlapping, leading to an increase of the darkening, that is, to a decrease of the gray level; for $E > 8 \times 10^9$ n cm^{-2} track overlapping becomes predominant and the darkening shows an approximately constant trend for a small interval (Ilic and Najzer, 1990a).

For 10 min the external ring area of the track is smaller than the one for 25 min (Fig. 5b) and according to the theory, the smaller the external ring area the greater the exposure to reach the same level of darkening. The obtained results agree with the theory since, as shown in Fig. 2, to reach the gray level GL = 230, for example, an exposure of $E \sim 4 \times 10^9$ n cm^{-2} for 10 min and $E \sim 1 \times 10^9$ n cm^{-2} for 25 min is necessary.

For 65 min the external ring area is greater than the one for 25 min (Fig. 5b) and the exposure to reach the same gray level GL = 230 is about two times smaller, that is, $E \sim 5 \times 10^8$ n cm^{-2}. It is also important to observe that the dynamic range for 65 min is smaller than for 25 min and this can be explained by considering that for 65 min the track overlapping starts earlier.

The theory of the image formation in SSNTD also states that the intrinsic unsharpness reaches the minimal value $U_i \sim 0.8 \times R$ (where R is the range of the α-particle in the converter screen) for external ring diameters smaller than R and remains at this value while track overlapping is not predominant (Ilic and Najzer, 1990d). As the resolution was evaluated in those same experimental conditions for which the best contrast was achieved (1), the external ring diameter is smaller than R and the track overlapping is not predominant. Furthermore, taking into account that for the present screen $R \sim 10$ μm, the minimal theoretical value for the intrinsic unsharpness is $U_i \sim 8$ μm. As evaluated in our previous work, the minimal experimental value for the intrinsic unsharpness was $U_i \sim 17$ μm and the discrepancy between the theoretical and experimental values was attributed to the contact irregularities at the SSNTD/sample/screen interface and to the neutron beam and screen inhomogeneities (Pugliesi and Pereira, 2002). Since the obtained experimental value for the total unsharpness was $U_t = 23$ μm it is possible to conclude that there is an appreciable contribution of U_g in U_t even for the present experimental condition in which the SSNTD, the sample and the screen are

Fig. 7. Radiography of a fingerprint (etching 25 min; exposure 8×10^9 n cm^{-2}).

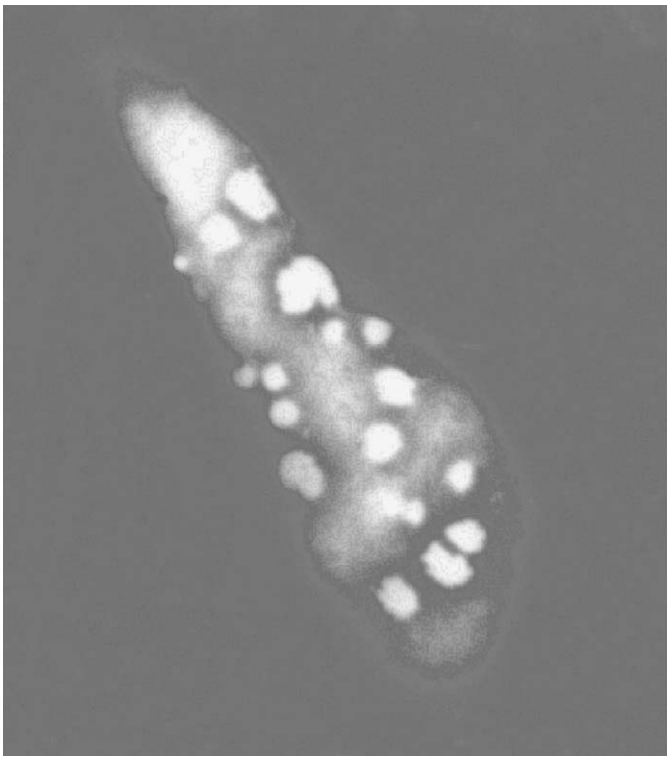

Fig. 8. Radiography of a bacteria colony (etching 25 min; exposure 8×10^9 n cm^{-2}).

kept in close contact during irradiation (2) and for a sample thickness of 10 μm.

4. Conclusions

The NIAR is a promising technique to inspect the internal structure of thin samples with thickness in the μm range. If a standard neutron radiography facility is available, the involved costs to have the method operational are very low because most of the infrastructure, such as the neutron beam, shielding, converter screens, cassettes, can be used. In order to demonstrate some possible applications of the method, Figs. 6–8 show the radiographs of a mice brain tissue 9 μm thick, fingerprint and of a bacteria colony, in which the image visualization was enhanced by digital processing.

When compared to the other radiography techniques, the present one exhibits two important characteristics: the first is a lower irradiation time to obtain the radiography (Belanger and Belanger, 1959) and the second the detector is not sensitive to gamma radiation enabling the inspection of radioactive samples or to perform radiographs in neutron beams having high gamma radiation content (Dhairyawan et al., 2003; Zaki and Seddik, 2007).

References

Belanger, L.F., Belanger, C., 1959. Alpha radiography: a simple method for determination of mass concentration in cells and tissues. J. Biophys. Biochem. Cytol. 6 (2), 197–205.

Dhairyawan, M.P., Marathe, P.K., Massand, O.P., 2003. Use of CR-39 solid state nuclear track detector in neutron personnel monitoring. Radiat. Meas. 36, 435–438.

Durrani, S.A., Bull, R.K., 1987. Solid state nuclear track detection. Principles, methods and applications. Int. Ser. Nat. Philos. 111. Pergamon Press.

Hardt, P. von Der, Roettger, H., 1981. Neutron Radiography Handbook: Nuclear Science and Technology. D. Reidl, Dordrecht.

Harms, A.A., Zellinger, A.A., 1977. New formulation of total unsharpness in radiography. Phys. Med. Biol. 22 (1), 70–80.

Ilic, R., Najzer, M., 1990a. Image formation in track-etch detectors—I. The Large area signal transfer function. Nucl. Track Radiat. Meas. 17, 453–460.

Ilic, R., Najzer, M., 1990b. Image formation in track-etch detectors—II. The Space-dependent transfer function in thin detectors. Nucl. Track Radiat. Meas. 17, 461–468.

Ilic, R., Najzer, M., 1990c. Image formation in track-etch detectors—III. The Space-dependent transfer function in thick detectors. Nucl. Track Radiat. Meas. 17, 469–473.

Ilic, R., Najzer, M., 1990d. Image formation in track-etch detectors—IV. Image quality. Nucl. Track Radiat. Meas. 17 (4), 475–481.

Pereira, M.A.S., 2007. Neutron induced alpha radiography. Ph.D. Thesis, IPEN-CNEN/SP.

Pugliesi, R., Pereira, M.A. Stanojev, Moraes, M.A.P.V., Menezes, M.O., 1999. Characteristics of the solid state nuclear detector CR-39 for neutron radiography purposes. Appl. Radiat. Isot. 50, 375–380.

Pugliesi, R., 2001. Progress of neutron radiography at the IEA-R1 nuclear research reactor (last 15 years). In: Meeting of the advisory group of development and application of neutron radiography. International Atomic Energy Agency (IAEA), Vienna.

Pugliesi, R., Pereira, M.A.S., 2002. Study of the neutron radiography characteristics for the solid state nuclear track detector Makrofol-DE. Nucl. Instrum. Methods Phys. Res. (A) 484, 613–618.

Pugliesi, R., Andrade, M.L.G., Pereira, M.A.S., Pugliesi, F., 2005. Neutron induced electron radiography. Nucl. Instrum. Methods A 542 (1–3), 81–86.

Wrobel, M., Greim, L., 1988. Resolution functions and unsharpness in neutron radiography. Geesthacht, German, GKSS (GKSS 88/e/12).

Zaki, M.F., Seddik, U., 2007. Changes produced in etching parameters of CR-39 by high dose pre- and post-irradiation. Radiat. Eff. Defects Solids 162 (6), 449–453.